AIAA JOURNAL
Vol. 32, No. 2, February 1994

Asymptotic Theory of Supersonic Propeller Noise

Edmane Envia*
Sverdrup Technology, Inc., Brook Park, Ohio 44142

An asymptotic theory for predicting noise radiation from supersonic propellers with realistic blade geometries is presented. The theory, which utilizes a large-blade-count approximation, provides simple closed-form expressions for the radiation efficiency integrals of all three types of propeller noise sources. Comparisons with a method that uses numerical integration of the radiation efficiency integrals indicate that sound levels predicted by the asymptotic theory are quite accurate. Asymptotic calculations also confirm the conclusions by earlier investigators that for high-speed propellers the noise radiated by the Lighthill quadrupole source is substantial when compared with the noise radiated by blade thickness and loading sources. Furthermore, the theory predicts that the propeller peak sound pressure level (SPL) increases monotonically below a critical tip helical Mach number but reaches a plateau and does not increase further above that critical Mach number. Both the predicted SPL trend and critical Mach number are in good agreement with experimental observations.

Nomenclature

Ai, Ai' = Airy function and its derivative
B = propeller blade count
c_0 = ambient speed of sound
e_j = unit vector along radiation direction
f = amplitude of blade aerodynamic loading
$G(\boldsymbol{x}, t/\boldsymbol{y}, \tau)$ = free-space moving-medium Green's function
J = propeller advance ratio
M_R = source relative Mach number in the radiation direction
M_{tip} = blade tip rotational Mach number
M_{tip_h} = relative tip helical Mach number
M_{0_j} = freestream Mach number
n_j = outward surface unit normal
p = local fluid pressure
$p'(\boldsymbol{x}, t)$ = acoustic pressure
$p_l(\boldsymbol{x})$ = Fourier harmonic component of acoustic pressure
$Q^{\ell}_{\ldots}$ = acoustic source strength
R = distance between observer and source
r = radial coordinate
$S(\tau)$ = propeller blade surface(s)
T_{jk} = inviscid Lighthill stress tensor
t = observer time
U_{0_j} = freestream velocity
u_j = local fluid velocity
$V(\tau)$ = volume exterior to propeller blades
v_n = normal component of blade surface velocity
x_j = observer Cartesian coordinates
y_j = source Cartesian coordinates
α = propeller angle of attack
Δ = elemental area/volume
δ = Dirac delta function
δ_{jk} = Kronecker delta
ρ = local fluid density
τ = source (i.e., retarded) time
$\Phi(\theta)$ = propeller phase function
φ = angular coordinate
Ψ_C = convective phase factor
Ω = propeller angular speed

Subscripts

0 = ambient condition
$\mathfrak{L}$ = loading noise component
$\mathfrak{Q}$ = quadrupole noise component
s = typical surface/volume element
$\mathfrak{T}$ = thickness noise component

Introduction

OVER the last dozen years, renewed interest in supersonic propeller (propfan) technology and the drive to meet stringent community and cabin noise regulations have spurred a great deal of theoretical and experimental research activity in the area of high-speed rotor noise. On the theoretical side, in particular, significant strides have been made toward the development of accurate theories for predicting supersonic propeller noise. The foundation for many of these theories has been the Ffowcs Williams and Hawkings[1] (FW-H) equation, which provides a theoretical basis for calculating the radiation of sound from the propeller blade surfaces (i.e., the thickness and loading noise) as well as the sound generated by the flowfield surrounding the propeller disk (i.e., the Lighthill quadrupole noise). The noise generated by thickness and loading sources has received a great deal of attention as exemplified by the theories of Hanson[2] and Farassat.[3] In contrast, most of the research in the area of propeller quadrupole noise has been of an exploratory nature (see, for example, Hanson and Fink[4]), even though conclusions from these efforts have suggested that quadrupole radiation could be potentially significant for supersonic rotors. Recent work by Peake and Crighton,[5] however, has reinforced the notion that quadrupole radiation must be accounted for in predicting the noise generated by high-speed propellers.

From a computational point of view, prediction of propeller noise involves evaluation of the multiple integrals appearing in the FW-H equation. This task can be accomplished by various methods, but, in general, an accurate and detailed prediction requires the use of numerical integration (i.e., an appropriate quadrature scheme). That, in turn, necessitates the utilization of a large number of source points to create a realistic representation of the propeller geometry as well as the flowfield surrounding it. In practice, the number of thickness and loading sources necessary for such a representation is sufficiently small to make the computation of radiated noise by these two types of sources feasible. In contrast, the substantially larger number of quadrupole sources needed for a faithful representation of the flowfield around a propeller disk makes quadrupole noise computations considerably less viable. Although the application of various simplification schemes like the far-field

Presented as Paper 92-02-064 at the DGLR/AIAA 14th Aeroacoustics Conference, Aachen, Germany, May 11–15, 1992; received Nov. 20, 1992; revision received June 11, 1993; accepted for publication June 18, 1993.

*Senior Research Engineer, 2001 Aerospace Parkway. Member AIAA.

approximation has yielded some measure of success, a realistic calculation has, for the most part, remained computationally expensive.

An appealing method for circumventing this problem, first suggested by Hawkings and Lowson[6] in the context of a frequency-domain analysis, is the use of the large-blade-count approximation to calculate the source distribution integrals appearing in the FW-H equation asymptotically. For modern, many-bladed propfan designs this approach offers a very effective alternative to direct numerical integration. The effectiveness of this approach was demonstrated by Crighton and Parry,[7] who developed an asymptotic theory for propeller thickness and loading noise radiation. In fact, this theory was also used by the authors in Ref. 5 to assess the importance of propeller quadrupole noise. To date, however, the published results of this theory have been limited to propellers with fairly simple geometries. Therefore, as it stands, there is a gap between the theories that use numerical integration and can accommodate realistic blade geometries but are rather unwieldy for calculating noise radiation from quadrupole sources and the asymptotic theory described in Refs. 5 and 7, which is quite efficient for quadrupole noise calculations but, so far, is restricted to simple geometries.

The theory presented in this paper bridges that gap. It uses a large-blade-count approximation to evaluate integrals in the FW-H equation. But, unlike Refs. 5 and 7, the "asymptotics" are applied to the radiation efficiency integrals instead of the source distribution integrals. This approach affords the flexibility of using realistic blade geometries while keeping the computer time requirements small. The asymptotic analysis for thickness and loading noise sources was presented by Envia[8] and was shown to provide very good agreement with numerical integration. The theory is now extended to include quadrupole noise. Therefore, for the sake of completeness the full analysis will be detailed here. Comparisons with results computed using numerical integration will then be shown and an application of the theory to a practical problem of interest will be presented. Finally, predictions from this theory will be compared with those from other theories.

Analysis

The starting point for the analysis is Goldstein's[9] version of the FW-H equation for the acoustic pressure $p'(\boldsymbol{x}, t)$ written in the propeller-fixed (wind-tunnel) coordinate system:

$$p'(\boldsymbol{x},t) = -\int_{-\infty}^{+\infty}\int_{S(\tau)} \rho_0 v_n \frac{\mathrm{D}_0 G}{\mathrm{D}\tau}\,\mathrm{d}s(\boldsymbol{y})\,\mathrm{d}\tau + \int_{-\infty}^{+\infty}\int_{S(\tau)} f n_j \frac{\partial G}{\partial y_j} \times \mathrm{d}s(\boldsymbol{y})\,\mathrm{d}\tau + \int_{-\infty}^{+\infty}\int_{V(\tau)} T_{jk}\frac{\partial^2 G}{\partial y_j \partial y_k}\,\mathrm{d}\boldsymbol{y}\,\mathrm{d}\tau \tag{1a}$$

$$T_{jk} = \rho u_j u_k + \delta_{jk}\left[(p-p_0) - c_0^2(\rho-\rho_0)\right] \tag{1b}$$

$$\frac{\mathrm{D}_0}{\mathrm{D}\tau} = \frac{\partial}{\partial\tau} + U_{0_j}\frac{\partial}{\partial y_j} \tag{1c}$$

where the velocities u_j and v_n are given relative to a medium-fixed coordinate system, even though Eq. (1a) is expressed in a propeller-fixed coordinate system. It should be noted that the convention for the direction of unit normal is opposite that of Goldstein's. The freestream velocity U_{0_j} is equal to and negative of the propeller forward-flight velocity. Note that, as given earlier, T_{jk} represents only the inviscid part of the Lighthill stress tensor. For a propeller, the viscous contribution to the stress tensor is essentially negligible in nearly all applications of practical interest. The three terms in Eq. (1a) represent contributions from the thickness, loading, and Lighthill stress (quadrupole) sources of propeller noise, respectively.

It can be shown that the Green function in Eq. (1a) has the following form:

$$G = \frac{1}{4\pi\kappa R}\,\delta(t-\tau-g_c R/c_0) \tag{2a}$$

$$g_c(\tau) = \frac{1}{\beta_0^2}(\kappa - M_{0_R}), \qquad \kappa(\tau) = (M_{0_R}^2 + \beta_0^2)^{1/2} \tag{2b}$$

$$M_{0_R}(\tau) = M_{0_j} e_j, \qquad \beta_0 = (1-M_{0_j}^2)^{1/2} \quad \text{(sum over } j\text{)} \tag{2c}$$

$$M_{0_j} = \frac{U_{0_j}}{c_0}, \qquad e_j(\tau) = \frac{(x_j - y_j)}{R}, \qquad R(\tau) = |\boldsymbol{x} - \boldsymbol{y}(\tau)| \tag{2d}$$

where parameters g_c and κ represent the effects of medium convection on the retarded time and spherical spreading rate, respectively. The explicit dependence of various parameters on source time τ is indicated where necessary.

In general, because the propeller may be operating at an angle of attack to the oncoming flow, the 1-axis is chosen to coincide with the propeller shaft (see Fig. 1) to simplify the description of the source motion. As a result, motion of the sources is confined to the transverse planes described by the 2- and 3-axes. Therefore, as depicted in Fig. 1, it can be readily seen that

$$M_{0_1} = M_0\cos\alpha, \qquad M_{0_2} = 0, \qquad M_{0_3} = M_0\sin\alpha \tag{3}$$

It should be noted that Hanson and Parzych[10] have developed a similar moving-medium formulation in connection with propellers operating in angular inflow. They, however, have formulated the problem in a coordinate system aligned with the flow instead of one aligned with the propeller axis. The choice of coordinate system is entirely arbitrary and only affects the final form of the working expressions. The form chosen by the authors in Ref. 10 simplifies the numerical integrations that are performed in their analysis. The choice made in this paper serves to facilitate the asymptotic analysis that will be carried out once the desired form of the FW-H equation is derived.

Provided that the blade geometry, aerodynamic loading, and flowfield about the propeller are known in sufficient detail, acoustic pressure $p'(\boldsymbol{x}, t)$ may be computed directly from Eq. (1a) for any observer location. This, of course, is the so-called time-domain approach that entails solving transcendental equations for source time τ. Alternatively, one can use the frequency-domain approach, which involves expanding $p'(\boldsymbol{x}, t)$ in terms of its Fourier harmonic components $p_l'(\boldsymbol{x})$, i.e.,

$$p'(\boldsymbol{x},t) = \sum_{l=-\infty}^{+\infty} p_l'(\boldsymbol{x}) e^{-il\Omega t} \tag{4a}$$

with the individual harmonic components given by

$$p_l'(\boldsymbol{x}) = p_{3_l}'(\boldsymbol{x}) + p_{\mathfrak{L}_l}'(\boldsymbol{x}) + p_{\mathfrak{Q}_l}'(\boldsymbol{x}) \tag{4b}$$

where

$$p_{3_l}'(\boldsymbol{x}) = \frac{\Omega}{2\pi}\int_0^{2\pi/\Omega} e^{il\Omega t}\left[\int_{-\infty}^{+\infty}\int_{S(\tau)} \rho_0 v_n \frac{\mathrm{D}_0 G}{\mathrm{D}t}\,\mathrm{d}s(\boldsymbol{y})\,\mathrm{d}\tau\right]\mathrm{d}t \tag{4c}$$

$$p_{\mathfrak{L}_l}'(\boldsymbol{x}) = -\frac{\Omega}{2\pi}\int_0^{2\pi/\Omega} e^{il\Omega t}\left[\int_{-\infty}^{+\infty}\int_{S(\tau)} f n_j \frac{\partial G}{\partial x_j}\,\mathrm{d}s(\boldsymbol{y})\,\mathrm{d}\tau\right]\mathrm{d}t \tag{4d}$$

$$p_{\mathfrak{Q}_l}'(\boldsymbol{x}) = \frac{\Omega}{2\pi}\int_0^{2\pi/\Omega} e^{il\Omega t}\left[\int_{-\infty}^{+\infty}\int_{V(\tau)} T_{jk}\frac{\partial^2 G}{\partial x_j \partial x_k}\,\mathrm{d}\boldsymbol{y}\,\mathrm{d}\tau\right]\mathrm{d}t \tag{4e}$$

where $2\pi/\Omega$ represents one period of propeller revolution. These equations denote contributions to p_l' from the thickness, loading, and quadrupole sources, respectively. In writing Eqs. (4c-4e), the derivatives of G with respect to source coordinates from Eq. (1a) have been replaced by its derivatives with respect to observer coordinates through the use of the relations

$$\frac{\partial G}{\partial y_j} = -\frac{\partial G}{\partial x_j}, \qquad \frac{\mathrm{D}_0 G}{\mathrm{D}\tau} = -\frac{\mathrm{D}_0 G}{\mathrm{D}t} \tag{5}$$

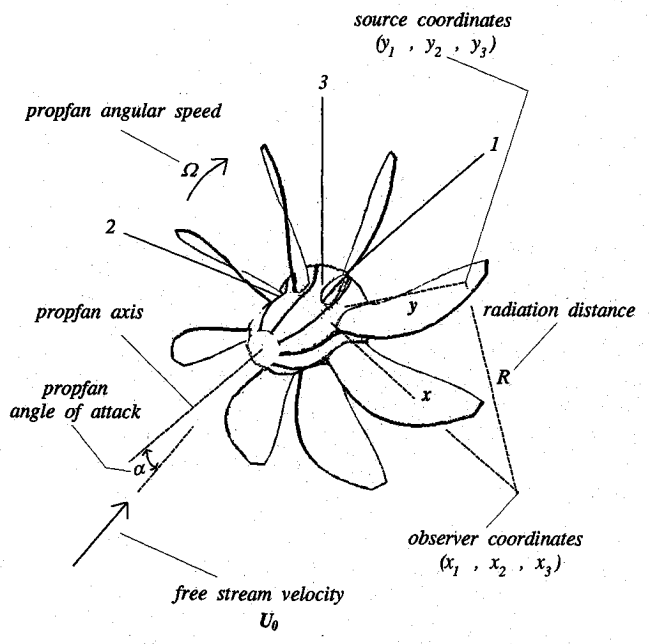

Fig. 1 Geometry and coordinate system.

This is done to facilitate the removal of the temporal derivatives in the FW-H equation as will be shown shortly. Using the usual phase relationship arguments it can be shown that, given B identical blades, only harmonic components for which $l = mB$ (where m is an integer) contribute to the infinite sum in Eq. (4a). This contribution is simply B times the contribution of a single blade. Therefore, from here on B will explicitly appear in expressions for the harmonic components $p'_{\mathfrak{I}mB}$, $p'_{\mathfrak{L}mB}$, and $p'_{\mathfrak{Q}mB}$. Correspondingly, S and V, respectively, will denote surface of and volume around a single blade.

To further simplify Eqs. (4c–4e) the spatial derivatives $\partial/\partial x_j$ and $\partial^2/\partial x_j \partial x_k$ of G may be rewritten in terms of the temporal derivative $\partial/\partial t$ through the use of the chain rule:

$$\frac{\partial G}{\partial x_j} = \mathfrak{D}_j(t)G \tag{6a}$$

$$\frac{\partial^2 G}{\partial x_j \partial x_k} = \left[\frac{\partial \mathfrak{D}_k(t)}{\partial x_j} + \mathfrak{D}_j(t)\mathfrak{D}_k(t)\right]G \tag{6b}$$

$$\mathfrak{D}_j(t) = -\left[\frac{1}{c_0\kappa}(e_j - g_c M_{0_j})\frac{\partial}{\partial t} + \frac{1}{\kappa^2 R}(\beta_0^2 e_j + M_{0_R} M_{0_j})\right] \tag{6c}$$

where the auxiliary derivative operator $\mathfrak{D}_j(t)$ has been introduced for notational brevity. The temporal derivatives can now be removed using integration by parts, and the integral over t, which involves a function, can be evaluated easily to yield

$$p'_{\mathfrak{I}mB}(\boldsymbol{x}) = \frac{B\Omega}{8\pi^2}\int_0^{2\pi/\Omega}\int_{S(\tau)}\left(\sum_{\ell=1}^{2}\frac{Q_{\mathfrak{I}}^{(\ell)}}{R^\ell}\right) \times \exp[imB\Omega(\tau + g_c R/c_0)]\, ds(\boldsymbol{y})\, d\tau \tag{7a}$$

$$p'_{\mathfrak{L}mB}(\boldsymbol{x}) = \frac{B\Omega}{8\pi^2}\int_0^{2\pi/\Omega}\int_{S(\tau)}\left(\sum_{\ell=1}^{2}\frac{Q_{\mathfrak{L}}^{(\ell)}}{R^\ell}\right) \times \exp[imB\Omega(\tau + g_c R/c_0)]\, ds(\boldsymbol{y})\, d\tau \tag{7b}$$

$$p'_{\mathfrak{Q}mB}(\boldsymbol{x}) = \frac{B\Omega}{8\pi^2}\int_0^{2\pi/\Omega}\int_{V(\tau)}\left(\sum_{\ell=1}^{3}\frac{Q_{\mathfrak{Q}}^{(\ell)}}{R^\ell}\right) \times \exp[imB\Omega(\tau + g_c R/c_0)]\, d\boldsymbol{y}\, d\tau \tag{7c}$$

where source strengths $Q^{(\ell)}_{\ldots}$s for each source type are organized according to which power of radiation distance R they multiply. Note also that the limits on the integration over τ have been changed to reflect the fact that an interval of size $2\pi/\Omega$ in t is mapped exactly into an interval of size $2\pi/\Omega$ in τ. The expressions for source strengths are given by

$$Q_{\mathfrak{I}}^{(1)} = -\frac{1}{\kappa^2} imB\Omega\rho_0 v_n\left[1 - \frac{1}{\kappa}M_{0_j}(e_j - g_c M_{0_j})\right] \tag{8a}$$

$$Q_{\mathfrak{I}}^{(2)} = -\frac{1}{\kappa^3}\rho_0 v_n M_{0_j}(\beta_0^2 e_j + M_{0_R} M_{0_j}) \tag{8b}$$

$$Q_{\mathfrak{L}}^{(1)} = -\frac{1}{c_0\kappa^2} imB\Omega f n_j (e_j - g_c M_{0_j}) \tag{8c}$$

$$Q_{\mathfrak{L}}^{(2)} = \frac{1}{\kappa^3} f n_j (\beta_0^2 e_j + M_{0_R} M_{0_j}) \tag{8d}$$

$$Q_{\mathfrak{Q}}^{(\ell)} = \frac{1}{\kappa^{\ell+2}} T_{jk}\left[\mathfrak{A}_1^{(\ell)}\delta_{jk} + \mathfrak{A}_2^{(\ell)} e_j e_k + \mathfrak{A}_3^{(\ell)} M_{0_j} M_{0_k} + \mathfrak{A}_4^{(\ell)}(e_j M_{0_k} + M_{0_j} e_k)\right], \qquad \ell = 1, 2, 3 \tag{8e}$$

$$\mathfrak{A}_1^{(1)} = 0, \quad \mathfrak{A}_2^{(1)} = 1, \quad \mathfrak{A}_3^{(1)} = g_c^2, \quad \mathfrak{A}_4^{(1)} = -g_c$$

$$\mathfrak{A}_1^{(2)} = -\kappa^2, \quad \mathfrak{A}_2^{(2)} = 3\beta_0^2, \quad \mathfrak{A}_3^{(2)} = -(1 + 2M_{0_R} g_c)$$

$$\mathfrak{A}_4^{(2)} = 2M_{0_R} - \beta_0^2 g_c \tag{8f}$$

$$\mathfrak{A}_1^{(3)} = -\beta_0^2\kappa^2, \quad \mathfrak{A}_2^{(3)} = 3(\beta_0^2\kappa^2 - M_{0_R}^2)$$

$$\mathfrak{A}_3^{(3)} = (3M_{0_R}^2 - \kappa^2), \quad \mathfrak{A}_4^{(3)} = 3\beta_0^2 M_{0_R}$$

where sums over the indices j and k are assumed. It should be noted that, in general, v_n, f, and T_{jk} depend on τ.

Once source strength distributions $Q^{(\ell)}_{\ldots}$ are estimated, what remains is to carry out the integrations in Eqs. (7a–7c). Ordinarily, the order of integration in these equations is reversed and the integral over τ, which represents the radiation efficiency of the acoustic source, is computed first. Since for general geometries and source strengths this integral is not tractable analytically, it is usually computed approximately for near- or far-field observer locations for which the integrand may be significantly simplified. The result is given in terms of the appropriate Bessel functions. The remaining surface (or volume) integral is then carried out using a quadrature scheme. Alternatively, as was mentioned earlier, the surface (or volume) integral may be calculated asymptotically in the manner suggested in Ref. 6. In this approach, which is particularly useful when the blade count B (or more appropriately the parameter mB) is large, the method of stationary phase is utilized to show that, asymptotically, most of the radiation from the blade surface (or the volume surrounding it) originates from the neighborhood of special points called the stationary phase points. As was pointed out in the introduction, this approach forms the basis of the theory presented in Refs. 5 and 7. The utility of this approach hinges on determining, analytically, the stationary phase points, which is a difficult task when dealing with blades having complicated geometries.

This difficulty, however, can be circumvented by applying the large-blade-count approximation to the integral over τ. In other words, the idea is to find the radiation efficiency of each source asymptotically. This is accomplished by evaluating the τ integral using a modification to the standard steepest descent and saddle-point methods. The advantage of this approach is that it is applicable to general geometries.

In this paper the derivation for the zero angle-of-attack case ($\alpha = 0$) will be outlined. The extension to nonzero angle of attack follows the analysis described in Ref. 8. For the sake of brevity the final formula will be given in terms of a generic source strength Q and a generic radiation distance "factor" $\mathfrak{R}$.

The resulting expression is therefore applicable to any $Q_{\cdots}^{(\ell)}$ and R^{ℓ} dependence.

For practical considerations it is more convenient to preserve the order of integration in Eqs. (7a–7c) and carry out the surface (or the volume) integral first. To do so, we begin by dividing the blade surface (or the volume surrounding it) into a number of small surface (or volume) elements. Let that number be N and each element be indexed by the subscript s. If the typical elemental size is sufficiently small, the integrand may be assumed to be constant over the extent of the element, and thus the surface (or volume) integral may be approximated by some appropriate "mean value" of the integrand times the elemental surface area (or volume). If the mean value is chosen to be the value of the integrand at the geometric center of the element, designated y_s, the error in this approximation is $\mathcal{O}(L^2)$ for a given N where $L = |y - y_s|_{\max}$. Of course, the error could be made arbitrarily small by choosing a large enough N which would reduce the effective size of each element.

Therefore, the generic harmonic amplitude $\mathcal{P}'_{smB}(\boldsymbol{x})$ for a given element may be written as

$$\mathcal{P}'_{smB}(\boldsymbol{x}) \simeq \frac{1}{\Omega} \sum_{s=1}^{N} \Delta_s \exp(-imB\Psi_{C_s}) I_s \tag{9a}$$

$$I_s = \int_0^{2\pi} \frac{Q_s(\theta)}{\mathcal{R}_s(\theta)} \exp[mB\Phi_s(\theta)]\, d\theta \tag{9b}$$

$$\Phi_s(\theta) = i\left(\theta + a_s\sqrt{1 - b_s\cos\theta}\right) \tag{9c}$$

$$\theta = \Omega\tau + \varphi_s - \varphi, \qquad \Psi_{C_s} = \frac{M_{\text{tip}}M_{0_1}}{\beta_{0_1}^2}(x_1 - y_{1_s}) + \varphi_s - \varphi \tag{9d}$$

$$a_s = \frac{M_{\text{tip}}}{\beta_{0_1}\sqrt{\chi_s^2 + r^2 + r_s^2}}, \qquad b_s = \frac{2rr_s}{\chi_s^2 + r^2 + r_s^2} \tag{9e}$$

$$\chi_s = \frac{1}{\beta_{0_1}}(x_1 - y_{1_s}), \qquad \beta_{0_1} = (1 - M_{0_1}^2)^{1/2} \tag{9f}$$

where (x_1, x_2, x_3) and $(y_{1_s}, y_{2_s}, y_{3_s})$ have been replaced by their cylindrical polar counterparts (x_1, r, φ) and $(y_{1_s}, r_s, \varphi_s)$, respectively. Furthermore, the integration variable τ is now replaced by a new variable, θ. The convective phase factor Ψ_{C_s} represents the collection of phase terms that do not depend on τ. The tip rotational Mach number M_{tip} is equal to $R_{\text{tip}}\Omega/c_0$, and χ_s is a scaled axial distance between observer and source. To simplify the notation, the explicit dependence of various variables on y_s has been suppressed.

The canonical phase function for a propeller operating at zero angle of attack is $\Phi_s(\theta)$, with a_s and b_s representing a combination of geometric, convective, and kinematic factors. Note that in deriving $\Phi_s(\theta)$ no assumptions about the geometry of the propeller blade or the location of the observer have been made. For this reason, the subsequent results apply to arbitrary geometries and observer locations. In the previous expressions both observer and source spatial coordinates are nondimensionalized by the propeller tip radius R_{tip}. Note that $M_{0_1} = M_0$ for the zero angle-of-attack case.

For a typical propfan, $B = 8$. Thus, even for the blade-passing-frequency (BPF) tone (i.e., $m = 1$), the integrand in Eq. (9b) is highly oscillatory. Nallasamy et al.,[11] who considered only the thickness and loading noise contributions, employed a quadrature scheme (i.e., the Romberg integration) to calculate I_s. Unfortunately, accurate computation of higher harmonics requires an ever increasing quadrature resolution to capture the oscillatory nature of the integrand, and the increasing resolution can raise the computational cost substantially. The asymptotic evaluation of I_s for large mB, however, can be quite cost effective.

To carry out the asymptotic evaluation, the variable θ must be allowed to be complex and the integration path (i.e., [0, 2π]) must be deformed into an appropriate contour. Replacing θ with the complex variable $\nu = \theta + i\sigma$ leads to a phase function $\Phi_s(\nu)$ that is also complex. It is fairly straightforward to find the saddle points of $\Phi_s(\nu)$ [i.e., $\Phi'_s(\nu) = 0$] and the appropriate steepest descent contours. The easiest way to find the saddle points is to define an auxiliary variable $\xi = \cos\nu$ and rewrite $\Phi'_s(\nu) = 0$ in terms of ξ:

$$(a_s b_s/2)^2\xi^2 - b_s\xi + 1 - (a_s b_s/2)^2 = 0 \tag{10}$$

where a_s and b_s were defined in Eq. (9d). Equation (10) is quadratic in ξ and may readily be solved. Thus, for a given observer and source location, $\Phi_s(\nu)$ has, in general, two simple saddle points in the interval [0, 2π]. It can be shown that the form of the two roots depends on whether the component of the source relative Mach number in the radiation direction, M_R, is subsonic or supersonic. The two are a complex conjugate pair if $M_R < 1$ and are real if $M_R > 1$. When $M_R = 1$ (i.e., the "sonic condition") these two saddle points merge to give rise to a single, second-order saddle point. For a subsonic source, only one of the two saddle points lies on the appropriate steepest descent path, hence only that saddle point contributes to the integral. It should be noted that the integrand also has an infinite number of branch points coinciding with those of $\Phi_s(\nu)$, of which only four lie in the region of interest. A judicious choice of branch cuts guarantees that the contributions to the contour integral along branch cuts in the ν plane are exponentially small compared with the contributions from the neighborhood of saddle points. The location of the appropriate saddle points, branch cuts, and steepest descent contours for typical source locations are shown in Fig. 2. Note that the choice of the steepest descent path depends on whether M_R is less than, equal to, or greater than unity. Also shown in this figure are the auxiliary descent contours needed for deforming the original contour [0, 2π] into the steepest descent contour(s). Because of the periodicity of the integrand in θ, the contributions from these contours cancel each other exactly.

For a given observer location and operating condition, the asymptotic structure of I_s for a source with $M_R = 1$ is different from that for a source with $M_R \neq 1$. In fact, it is fairly easy to show that the asymptotic expansion is given in terms of the inverse one-third powers of the parameter mB for a "sonic" source and in terms of the inverse one-half powers of mB for a "nonsonic" one. Since there is no simple way of constructing a composite expansion from these two expansions to allow for a smooth transition through the sonic condition, they are not convenient to use. However, this difficulty may be avoided altogether by developing a uniform asymptotic expansion using a theorem derived by Chester et al.[12] The

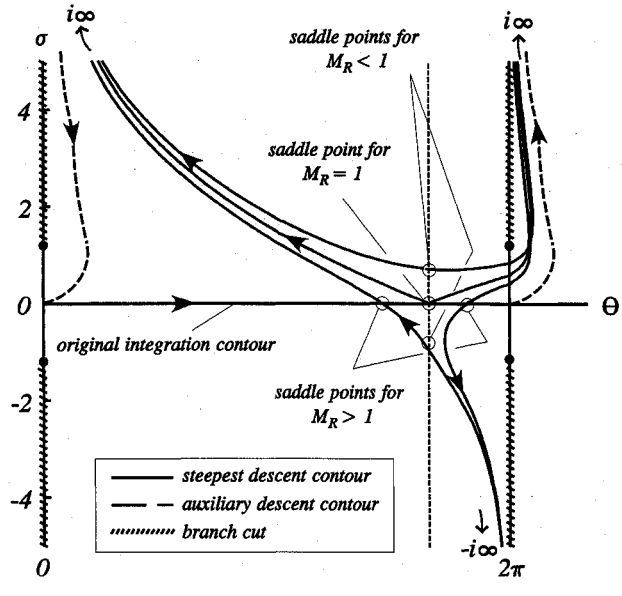

Fig. 2 Saddle points and steepest descent contours in the complex ν plane.

details of the methodology may be found in Bleistein and Handelsman.[13] The basic idea is to conformally map (say, $\nu \to \zeta$) the phase function $\Phi_s(\nu)$ into a much simpler function (i.e., a cubic polynomial) that exhibits the relevant features of the original phase function. The region of interest in the complex ν plane (i.e., the region containing saddle points and steepest descent contours) is correspondingly mapped into a region in the complex ζ plane. The standard steepest descent and saddle-point methods are then applied to the integral in the ζ plane. The key definitions and parameters, along with the final result, are summarized next.

The cubic is given by

$$\Phi_s(\nu) = -\left(\frac{\zeta^3}{3} - \gamma_s^2 \zeta\right) + \mu_s \tag{11a}$$

$$\mu_s = \tfrac{1}{2}\left[\Phi_s(\nu_s^+) + \Phi_s(\nu_s^-)\right] \tag{11b}$$

$$\gamma_s^3 = \tfrac{3}{4}\left[\Phi_s(\nu_s^+) - \Phi_s(\nu_s^-)\right] \tag{11c}$$

where ν_s^+ and ν_s^- denote the locations of saddle points of Φ_s in the complex ν plane, and μ_s and γ_s are parameters defining the conformal map. Note that γ_s as just given above can take on three possible values or branches. The theorem in Ref. 12 guarantees that one of the branches defines the desired conformal map. For integral I_s the branch chosen is the one for which γ_s^2 is purely real. With these parameters determined, the map can be constructed and the uniform asymptotic expansion carried out. In principle, the expansion of integral I_s could be developed to an arbitrary order in the parameter mB. However, it turns out that for most applications the first term provides a reasonable approximation even at BPF tone (i.e., $m = 1$). Therefore, in the subsequent analysis only the first term is retained.

After a fair amount of algebra the final result can be written as the following formula

$$I_s \simeq 2\pi i e^{mB\mu_s}\left\{d_{s_0}\frac{Ai\left[(mB)^{2/3}\gamma_s^2\right]}{(mB)^{1/3}} + d_{s_1}\frac{Ai'\left[(mB)^{2/3}\gamma_s^2\right]}{(mB)^{2/3}}\right\} \tag{12a}$$

$$d_{s_0} = \frac{\Gamma_0(\gamma_s) + \Gamma_0(-\gamma_s)}{2}, \quad d_{s_1} = \frac{\Gamma_0(\gamma_s) - \Gamma_0(-\gamma_s)}{2\gamma_s} \tag{12b}$$

$$\Gamma_0(\zeta) = \frac{Q_s\left[\nu(\zeta)\right]}{\Re_s\left[\nu(\zeta)\right]}\frac{d\nu}{d\zeta}, \quad \frac{d\nu}{d\zeta} = \frac{\gamma_s^2 - \zeta^2}{\Phi_s'\left[\nu(\zeta)\right]} \tag{12c}$$

where d_{s_0} and d_{s_1} are coefficients in the asymptotic expansion. It is worth mentioning that $\pm\gamma_s$ corresponds to the locations of saddle points $\nu_s^{\pm}$ in the ζ plane. For any observer location, the Airy function and its derivative provide a smooth transition from the blade region for which M_R is less than unity to the region for which M_R is greater than unity. For $\gamma_s = 0$ (i.e., a "sonic" source) Ai and Ai' are $\mathcal{O}(1)$, and consequently I_s is proportional to inverse one-third powers of mB. For $\gamma_s \neq 0$ (i.e., a "nonsonic" source) and large mB, Ai is $\mathcal{O}[(mB)^{-1/6}]$ and Ai' is $\mathcal{O}[(mB)^{1/6}]$. Consequently, I_s is proportional to the inverse one-half power of mB as expected. After substituting for I_s in Eq. (9a) from Eq. (12a) and adding the contributions from all of the N elements, the Fourier harmonic component $\mathcal{P}'_{mB}(\boldsymbol{x})$ can be calculated.

The appearance of the Airy function in asymptotic theories of sound radiation from high-speed propellers is not new. Crighton and Parry[14] used Airy functions to construct uniform higher order approximations for the large-index Bessel functions appearing in their asymptotic propeller noise theory. (Indeed, the Airy function is the natural choice for uniformizing asymptotic approximations used to describe certain transition phenomena in problems involving "high-frequency" wave propagation. See, for example, the problem of caustics in geometrical optics.[15]) The advantage of the present theory is that the evaluation of the radiation efficiency integral I_s yields the Airy function description in a natural and convenient way without the need for additional analysis such as that required in Ref. 14.

It should be noted here that the asymptotic approximation to the integral I_s, as given by Eqs. (12), is formally applicable only for high values of the parameter mB. The approximation suffers from loss of accuracy when mB becomes too small. This would be the case, for example, for the BPF tone of a two-bladed propeller for which $mB = 2$. This, of course, is not surprising since, as $mB \to 0$, the value of the integral is no longer dominated by the neighborhood of the saddle points, and the asymptotic approximation breaks down. However, even for a two-bladed propeller, the asymptotic formula can provide very good approximations at higher BPF harmonics (say, $m > 3$).

Results and Discussion

To assess the accuracy of the asymptotic formula given by Eq. (12a), we next consider its predictions for a test problem. The test case is that of a propfan operating at cruise conditions. The necessary aerodynamic input to the acoustic model is computed using an Euler computational fluid dynamics (CFD) code developed by Adamczyk (see Celestina et al.[16]) which provides both the loading distribution on propfan blades and the flowfield around the propfan. The CFD computations are for the flow conditions that roughly correspond to the wind-tunnel conditions in a series of acoustic measurements carried out at NASA Lewis Research Center by Dittmar and Stang[17] for a scale model SR-7A propfan operating at simulated cruise conditions. Unless otherwise noted, the acoustic calculations presented in this paper are for the BPF tone.

As was previously mentioned, the asymptotic formula is applicable to all three types of sources represented in Eqs. (7a–7c). The application of the formula to thickness and loading noise sources (i.e., surface sources) is quite straightforward since the spatial extent of their distribution is clearly defined. However, the "effective" spatial extent of the distribution of quadrupoles (i.e., volume sources) is not known a priori. To determine this effective spatial extent, a series of calculations employing the asymptotic formula for the quadrupole SPL was carried out using a series of progressively larger computational volumes surrounding the propfan blade.

The results of this study are shown in Fig. 3 where the predicted sideline directivity of quadrupole SPL for different computational volumes is plotted for near-field observer posi-

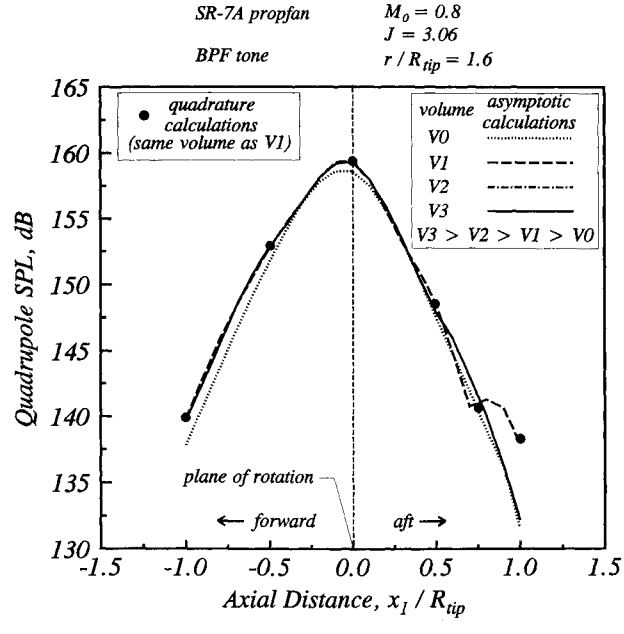

Fig. 3 Predicted sideline directivity of quadrupole source as a function of the computational volume chosen (asymptotic calculations).

tions located at a sideline distance of $r = 1.6\ R_{tip}$ from the axis of the propfan and extending from $1.0\ R_{tip}$ forward to $1.0\ R_{tip}$ aft of the plane of rotation. The freestream Mach number M_0 is 0.8, and the advance ratio J of the propfan is 3.06, which together result in a relative tip helical Mach number [i.e., $M_{tip_h} = (M_0^2 + M_{tip}^2)^{1/2}$] of 1.15. As a matter of convenience the computational volumes were chosen to coincide with the subsets of the CFD computational grid. In all, four volumes were considered. The passage volume, denoted $V0$, extends axially from the blade's leading edge to its trailing edge and extends radially from hub to tip. Volume $V1$ extends axially from the propeller plane of rotation [i.e., the (x_2, x_3) plane] to about 0.6 R_{tip}, volume $V2$ to 2.0 R_{tip}, and volume $V3$ to 4.0 R_{tip} in both the forward and aft directions. The latter three volumes also extend a distance of 0.5 R_{tip} beyond the blade tip in the radial direction. All four volumes also span the blade passage halfway to the adjacent blades in the circumferential direction on each side. For each volume the contributions to noise field from the Lighthill quadrupoles contained within the volume were computed and plotted.

Two important conclusions drawn from the plot in Fig. 3 are 1) that the predicted peak quadrupole SPL occurs in the vicinity of the plane of rotation and 2) that as far as the peak noise levels are concerned, volume $V1$ is optimally suited for acoustic calculations since the larger volumes produce levels that are generally no more than 1 dB different from those for volume $V1$. (The results for volumes $V2$ and $V3$ are virtually indistinguishable.) The erratic behavior of the predicted SPL for the baseline volume $V1$ at the axial observer locations aft of the 0.6 R_{tip} position is a result of the choice of the computational volume. Because these observer locations lie near the boundary between $V1$ and $V2$, in the baseline case they only receive contributions from sources located upstream of that boundary (i.e., those inside $V1$ only). Clearly, as the computational volume is extended and contributions from sources downstream of that boundary (i.e., those inside $V2$ but not inside $V1$) are also taken into account, more realistic levels are produced, and the "kink" in the SPL disappears. Furthermore, to verify that the kink is not an artifact of asymptotic calculations, a full numerical integration of the radiation efficiency integral for volume $V1$ was performed at a few discrete locations, and the results were plotted as solid symbols in Fig 3. The comparison between asymptotic and numerical calculations is strikingly good and serves to demonstrate the accuracy of asymptotic calculations.

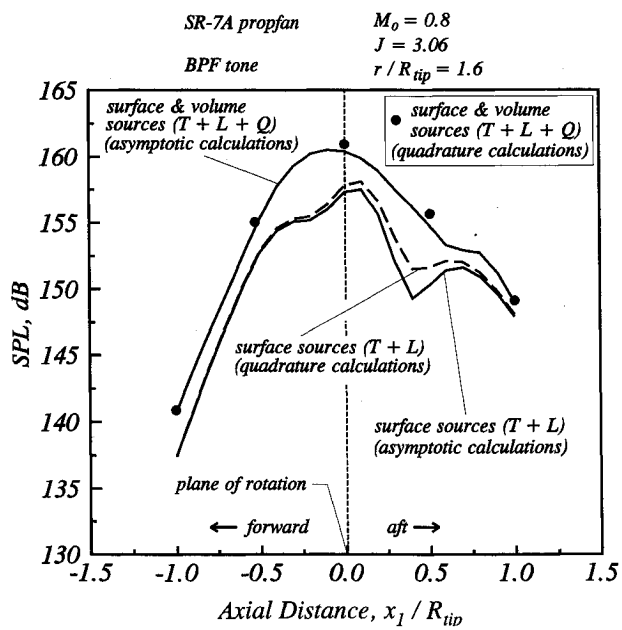

Fig. 4 Predicted sideline directivity; comparison of asymptotic and numerical results.

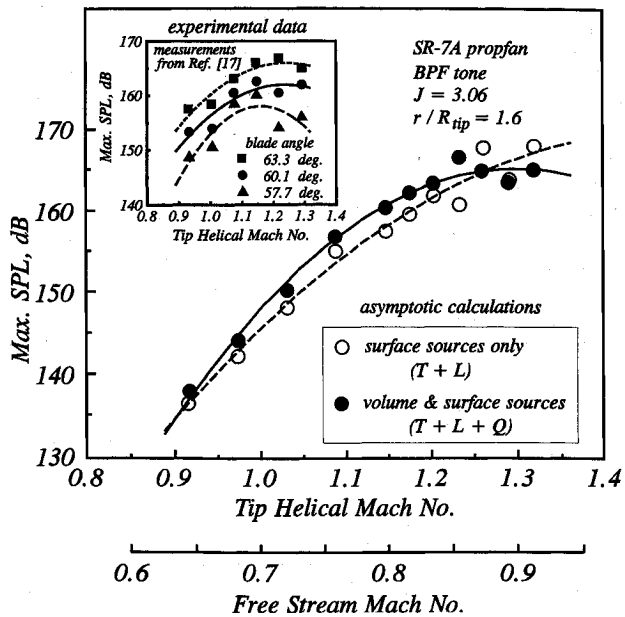

Fig. 5 Predicted variations of peak SPL with tip helical Mach number; inset: experimental data.

To further emphasize this accuracy, a comparison between the asymptotically and numerically computed sideline directivity of total SPL (thickness + loading + quadrupole) is presented in Fig. 4. The operating conditions and observer locations are the same as those in Fig. 3. The quadrupole contribution from volume $V1$ was considered in this comparison. The numerical integration was carried out for only five observer locations to limit the computational time. Again, the agreement is very good with deviations of less than 1 dB in the plane of rotation between asymptotic and numerical results. For comparison, the corresponding sideline directivity for the noise generated by surface (i.e., thickness + loading) sources is also shown. The agreement is quite good with a maximum deviation of about 2 dB occurring at about 0.5 R_{tip} downstream of the plane of rotation. A detailed examination of the individual source type contributions in this region revealed that on the one hand the discrepancy is partly due to deviations (of around 1 dB) between the asymptotically and numerically calculated loading noise predictions and on the other hand to the strong sensitivity of the sum of thickness and loading noise levels to their individual contributions. It is also interesting to note that there is noticeably higher total SPL as compared with that for surface sources, indicating that the quadrupole noise level is substantial for high-speed propellers and must be taken into account. This result reinforces the conclusions reached by the authors in Refs. 4 and 5 that the inclusion of quadrupole source contribution can substantially improve the theoretical predictions.

Comparison with Experimental Data

To demonstrate the utility of the present theory in providing answers to realistic problems, a series of acoustic calculations was performed to investigate the sensitivity of the maximum total SPL generated by a propfan as a function of its tip helical Mach number. The increase in M_{tip_h} was achieved by holding J constant (at 3.06) and increasing M_0. The range of tip helical Mach numbers studied was between 0.9 and 1.4 with 11 different Mach numbers considered within this range. The aerodynamic input in each case was computed using the Euler code mentioned earlier. As before, the computational volume chosen for acoustic calculations was $V1$. Twelve observer positions distributed on both sides of the plane of rotation were considered. These positions correspond to the microphone locations in Ref. 17. In each case the asymptotically computed peak total SPL was noted amongst observer

positions considered. In all cases this maximum occurred in the neighborhood of the plane of rotation.

The peak total SPL is plotted vs M_{tip_h} in Fig. 5. To see the trend, a quadratic curve is fitted to the predicted values (solid circles). The predicted trend indicates that maximum total SPL does not increase monotonically with increasing tip helical Mach number but rather "levels off" beyond M_{tip_h} of about 1.25. This behavior is consistent with the trends observed in the measurements reported in Ref. 17. As seen from the inset in Fig. 5, measured peak SPL generally reaches a plateau past $M_{\text{tip}_h} \simeq 1.25$. Different symbols in the inset represent peak SPLs corresponding to different propfan blade setting angles, whereas the lines are quadratic curve fits through the points.

In this paper no attempt was made to carry out a detailed comparison with the experimental data, due to the ambiguities that exist in matching the experimental operating conditions with their CFD counterparts. For the sake of comparison, however, the maximum SPL as predicted from only the surface sources is also plotted (open circles) in Fig. 5. It is interesting to note that, in contrast with total SPL, predicted peak SPL arising from surface sources tends to rise monotonically with the increasing tip helical Mach number. An examination of theoretical predictions revealed that the difference in behavior between peak SPLs may be traced to the mutual phase relationship between surface and volume sources. For $M_{\text{tip}_h} < 1.25$, surface and volume sources radiate essentially in phase. Therefore, they contribute additively to the total SPL. For $M_{\text{tip}_h} > 1.25$, however, surface and volume sources tend to radiate out of phase. This leads to mutual cancellation between the two types of sources and, as a result, in reduced peak total SPL.

Comparison with Other Theories

Unfortunately, it is rather difficult to compare quadrupole noise predictions from the present theory with those from other noise theories. This is either because predictions for quadrupole radiation from other theories are not readily available in the literature or because when such results are available it is very difficult to duplicated the flowfield that is necessary in quadrupole noise calculations. For these reasons, in this paper, comparison with other theories is limited to results for surface sources only.

To that end, in Fig. 6, the predicted spectra for thickness and loading from present asymptotic theory are compared with those from Farassat's time-domain theory and Hanson's helicoidal surface theory. The predictions are for the amplitudes of the first 10 BPF harmonics for an SR-3 propfan scale model in cruise condition. The predictions from Farassat's and Hanson's theories were taken from a report by Farassat et al.[18] (Predictions from Hanson's theory were available only for BPF.) The operating parameters and observer locations are denoted on the figure. It should be noted that the levels plotted in Fig. 6 are the free-field predictions. Therefore, those taken from Ref. 18 were reduced by 4 dB to provide the "uncorrected" levels.

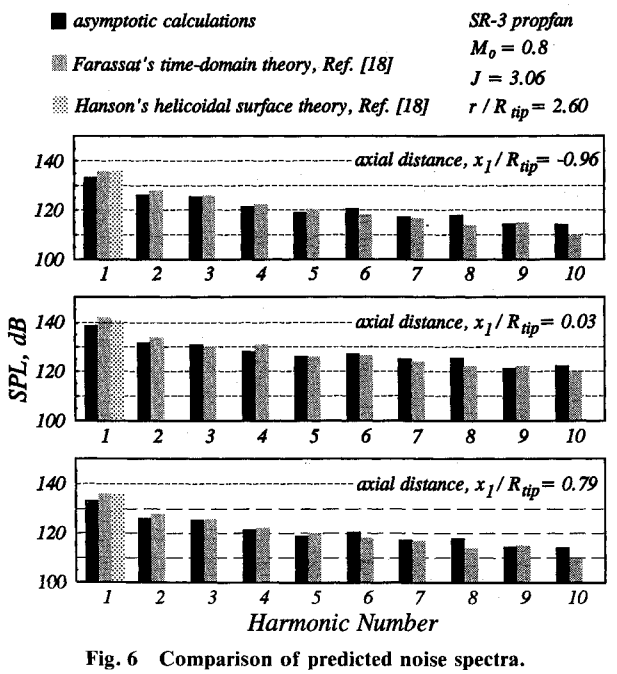

Fig. 6 Comparison of predicted noise spectra.

It should also be pointed out that only the input geometry to the three theories is identical. The aerodynamic loading input that is necessary for loading noise calculations is different (at least in its detail) in each case since, in general, it is not possible to duplicate, exactly, the aerodynamic loading distributions used by the other authors. Despite these input discrepancies, however, the levels predicted by the asymptotic theory differ slightly from those of Farassat's and Hanson's theories. These small differences, which are generally on the order of 2 dB, once again demonstrate the accuracy of the asymptotic theory.

It is worth mentioning that the CPU times required for the asymptotic noise calculations were generally an order of magnitude smaller than those necessary for numerical integration. Numerical integration was carried out using a Romberg quadrature scheme that automatically chooses the number of integration steps according to a prescribed criterion. This was adjusted to provide the desired accuracy with the minimum number of integration steps. The CPU time savings were even more significant for higher harmonics of BPF where numerical integration required a progressively finer quadrature step size. In contrast, asymptotic calculations incurred a nominal increase in CPU time over that required for the BPF tone calculations, since saddle-point locations are independent of the harmonic number. Furthermore, due to the very nature of the asymptotic expansion, predictions for higher harmonics are even more accurate when compared with numerical results (see Ref. 8). Naturally, the issue of CPU time savings is only relevant in the context of a frequency-domain analysis since in a time-domain approach all of the BPF harmonics are computed simultaneously. However, it should be noted that in a time-domain analysis this apparent advantage is offset by the necessity to solve a transcendental equation iteratively for the source time for each acoustic source under consideration.

Finally, it should also be mentioned that there are alternative approaches to the present theory, which are based not on the FW-H equation but on Kirchhoff's formula.[19] For example, Hawkings[20] proposed an approach in which the rotor is surrounded by a moving surface on which appropriate surface conditions (generally, pressure perturbation and normal velocity) are specified from nonlinear aerodynamic calculations within the surface. Outside of the surface then, the sound field is computed from these surface conditions through the use of a moving-surface version of Kirchhoff's formula. Although, in principle, this method is applicable to high-speed propeller noise, it can be computationally very expensive. This is because of the requirement that the surface be placed outside the nonlinear flow region. This requirement necessitates detailed nonlinear aerodynamic computations extending from the neighborhood of the propeller disk to the bounding Kirchhoff surface, which is an expensive proposition, especially since the pressure and velocity conditions on the surface should be specified with sufficient accuracy. Therefore, the issue of whether the computational effort involved in the use of Kirchhoff's formula is less than or more than that required by the asymptotic theory described in this paper is one that, unfortunately, cannot be answered a priori.

Concluding Remarks

A large-blade-count asymptotic theory that allows for the accurate and efficient calculation of the noise field of high-speed propellers was presented. The theory does not rely on the

simplifying assumptions usually employed in other propeller noise analyses. A closed-form expression involving the Airy function and its derivative gives a uniform representation of the noise field of a source regardless of whether its component of the relative Mach number in the radiation direction is less than, equal to, or greater than unity. The levels of all three types of propeller noise sources (i.e., thickness, loading, and Lighthill quadrupoles) were computed for a realistic propeller geometry and operating condition at a reasonable computational cost. Comparisons with numerical results and other theories demonstrate the accuracy of the asymptotic approximation. The results also indicate that near-field quadrupole radiation is substantial in the vicinity of plane of rotation and can significantly influence the total sound pressure level radiated by a supersonic propeller. The principal theoretical result of this paper is that, for a supersonic propeller, as the tip helical Mach number is increased, the maximum total SPL increases monotonically below a critical Mach number, but it levels off above that critical Mach number. Both the predicted SPL trend and the critical Mach number follow experimental measurements closely. Finally, the asymptotic theory presented in this paper is formally valid for high blade count and/or high harmonic order. When either of these parameters becomes so small that their product approaches zero, the approximation breaks down.

Acknowledgments

This work was supported under NASA Grant NAS3-25266 and carried out at NASA Lewis Research Center in Cleveland, Ohio. The author wishes to thank Osamu Yamamoto and John Papp for providing him with the computed flowfields.

References

[1]Ffowcs Williams, J. E., and Hawkings, D. L., "Sound Generation by Turbulence and Surfaces in Arbitrary Motion," *Philosopical Transactions of the Royal Society of London, Series A: Mathematical and Physical Sciences,* Vol. 264, May 1969, pp. 321–342.

[2]Hanson, D. B., "Near-Field Frequency-Domain Theory for Propeller Noise," *AIAA Journal,* Vol. 23, No. 4, 1985, pp. 499–504.

[3]Farassat, F., "Linear Acoustic Formulas for Calculation of Rotating Blade Noise," *AIAA Journal,* Vol. 19, No. 9, 1981, pp. 1122–1130.

[4]Hanson, D. B., and Fink, M. R., "The Importance of Quadrupole Sources in Prediction of Transonic Tip Speed Propeller Noise," *Journal of Sound and Vibration,* Vol. 62, Jan. 1979, pp. 19–38.

[5]Peake, N., and Crighton, D. G., "Lighthill Quadrupole Radiation in Supersonic Propeller Acoustics," *Journal of Fluid Mechanics,* Vol. 223, Feb. 1991, pp. 363–382.

[6]Hawkings, D. L., and Lowson, M. V., "Theory of Open Supersonic Rotor Noise," *Journal of Sound and Vibration,* Vol. 36, Sept. 1974, pp. 1–20.

[7]Crighton, D. G., and Parry, A. B., "Asymptotic Theory of Propeller Noise Part II: Supersonic Single-Rotation Propeller," *AIAA Journal,* Vol. 29, No. 12, 1991, pp. 2031–2037.

[8]Envia, E., "Prediction of Noise Field of a Propfan at Angle of Attack," NASA CR-189047, Oct. 1991; see also *Proceedings of the Sixth International Symposium on Unsteady Aerodynamics, Aeroacoustics and Aeroelasticity of Turbomachines and Propellers,* Springer-Verlag, Berlin, 1993, pp. 685-703.

[9]Goldstein, M. E., *Aeroacoustics,* McGraw-Hill, New York, 1976, pp. 189–192.

[10]Hanson, D. B., and Parzych, D. J. "Near Field Noise Theory for Propellers with Angular Inflow," DGLR/AIAA Paper 92-02-049, May 1992.

[11]Nallasamy, M., Envia, E., Clark, B. J., and Groeneweg, J. F., "Near-Field Noise of a Single Rotation Propfan at an Angle of Attack," AIAA Paper 90-3953, Oct. 1990; see also NASA TM-103645, Oct. 1990.

[12]Chester, C., Friedman, B., and Ursell, F., "An Extension of the Method of Steepest Descent," *Proceedings of the Cambridge Philosophical Society,* Vol. 54, 1957, pp. 599–611.

[13]Bleistein, N., and Handelsman, R. A., *Asymptotic Expansions of Integrals,* Dover, New York, 1986, pp. 369–374.

[14]Crighton, D. G., and Parry, A. B., "Higher Approximations in the Asymptotic Theory of Propeller Noise," *AIAA Journal,* Vol. 30, No. 1, 1992, pp. 23–28.

[15]Ludwig, D., "Uniform Asymptotic Expansions at a Caustic," *Communications on Pure and Applied Mathematics,* Vol. XIX, 1966, pp. 215–250.

[16]Celestina, M. L., Mulac, R. A., and Adamczyk, J. J., "A Numerical Simulation of the Inviscid Flow Through a Counterrotating Propeller," NASA TM-87200, June 1986.

[17]Dittmar, J. H., and Stang, D. B., "Cruise Noise of the 2/9 Scale Model of the Large-Scale Advanced Propfan (LAP) Propeller, SR-7A," NASA TM-100175, Sept. 1987.

[18]Farassat, F., Dunn, M. H., and Padula, S. S., "Advanced Turboprop Noise Prediction—Development of a Code at NASA Langley Based on Recent Theoretical Results," Final Report to NASA Lewis Research Center, June 1986, pp. 50–55.

[19]Dowling, A. P., and Ffowcs Williams, J. F., *Sound and Sources of Sound,* Ellis Horwood, Chichester, England, UK, 1983, pp. 174–175.

[20]Hawkings, D. L., "Noise Generation by Transonic Open Rotors," Westland Helicopter Ltd., Westland Research Paper 599, Yeovil, England, UK, 1979.